

Original Research

Multi-view prediction of Alzheimer's disease progression with end-to-end integrated framework



Yan Zhao^a, Baoqiang Ma^b, Tongtong Che^a, Qionglin Li^c, Debin Zeng^a, Xuotong Wang^a, Shuyu Li^{a,c,*}

^a Beijing Advanced Innovation Centre for Biomedical Engineering, School of Biological Science and Medical Engineering, Beihang University, Beijing, China

^b Department of Radiation Oncology, University of Groningen, Groningen, the Netherlands

^c State Key Lab of Cognition Neuroscience & Learning, Beijing Normal University, Beijing, China

ARTICLE INFO

Keywords:

Alzheimer's disease progression prediction
Cognitive score
Structural magnetic resonance image
Multi-task learning
Region-of-interest-attentive generative adversarial network

ABSTRACT

Alzheimer's disease is a common neurodegenerative brain disease that affects the elderly population worldwide. Its early automatic detection is vital for early intervention and treatment. A common solution is to perform future cognitive score prediction based on the baseline brain structural magnetic resonance image (MRI), which can directly infer the potential severity of disease. Recently, several studies have modelled disease progression by predicting the future brain MRI that can provide visual information of brain changes over time. Nevertheless, no studies explore the intra correlation of these two solutions, and it is unknown whether the predicted MRI can assist the prediction of cognitive score. Here, instead of independent prediction, we aim to predict disease progression in multi-view, i.e., predicting subject-specific changes of cognitive score and MRI volume concurrently. To achieve this, we propose an end-to-end integrated framework, where a regression model and a generative adversarial network are integrated together and then jointly optimized. Three integration strategies are exploited to unify these two models. Moreover, considering that some brain regions, such as hippocampus and middle temporal gyrus, could change significantly during the disease progression, a region-of-interest (ROI) mask and a ROI loss are introduced into the integrated framework to leverage this anatomical prior knowledge. Experimental results on the longitudinal Alzheimer's Disease Neuroimaging Initiative dataset demonstrated that the integrated framework outperformed the independent regression model for cognitive score prediction. And its performance can be further improved with the ROI loss for both cognitive score and MRI prediction.

1. Introduction

Alzheimer's disease (AD), the most common cause of dementia, is a neurodegenerative brain disease. Patients with AD suffer from progressive and irreversible deterioration of memory, cognition, and behavior until death [1]. In the year 2018, people with dementia is approximate to 50 million worldwide, and estimated to be 152 million by 2050 [2]. AD not only severely disturbs the normal daily living of patients and their families, but also causes heavy social and economic burdens [3]. Unfortunately, there is no pharmaceutical or clinical treatment available to stop or reverse the disease progression of AD [3]. Therefore, tracking AD progression is significantly important for enhancing the understanding of AD, monitoring the efficiency of new treatments or therapeutic interventions, and especially being beneficial for the early diagnosis [4].

Cognitive deterioration is a prominent symptom of AD. Various neuropsychological tests can be conducted to get the cognitive or clinical scores of subjects, which can reflect their cognitive functioning [5,6]. For example, mini mental state examination (MMSE) [7], a test including five cognitive areas to assess mental status, has been widely used for grading the cognitive state of AD patients [8]. Alzheimer's disease assessment scale cognitive subscale (ADAS-cog) [9], including eleven subject-completed tests and observer-based assessments, has been employed to measure cognition in patients with mild to moderate AD, which is considered as the gold standard for assessing the efficacy of antidementia treatments [10]. Those cognitive scores can be obtained easily and cheaply in clinical practice, and used as common clinical biomarkers for AD diagnosis. To some extent, the changing of cognitive score can reveal AD progression [11,12]. Thus, many approaches have formulated disease progression as the regression task by predicting the

* Corresponding author at: State Key Lab of Cognition Neuroscience & Learning, Beijing Normal University, Beijing, China.
E-mail address: shuyuli@bnu.edu.cn (S. Li).

<https://doi.org/10.1016/j.jbi.2021.103978>

Received 21 July 2021; Received in revised form 5 December 2021; Accepted 11 December 2021

Available online 16 December 2021

1532-0464/© 2021 Elsevier Inc. All rights reserved.

future cognitive score, based on baseline magnetic resonance image (MRI) [13–21]. For example, Jiang *et al.* [17] have calculated brain features (e.g., cortical volume and thickness) from structural MRI at baseline and then used them to predict future MMSE and ADAS-cog scores. Bhagwat *et al.* [19] have adopted an anatomically partitioned artificial neural network to extract features from the hippocampus region and cortical surface of baseline MRI, and then predict the clinical score at one year later. These feature-based prediction methods may confront some issues, such as which features should be extracted, how to perform feature selection and dimensionality reduction, and which regression algorithm to be selected [22]. Deep learning [23] can overcome these problems and has shown promising performance in the field of medical image analysis [24–26]. Lian *et al.* [27] have proposed an end-to-end deep learning model for the joint regression of multiple cognitive scores from baseline structural MRI. Yet, it still remains challenging to predict future cognitive score automatically and precisely.

Compared with cognitive decline, the brain structural changes associated with AD may appear much earlier, which can be detected by structural MRI [3,28]. This high-dimensional image carries more complementary, visualized and interpretable information than the cognitive score. In clinical diagnosis, medical experts would not make any decision before checking MRI scan of patient, revealing the significant role of MRI in tracing AD progression [29]. Therefore, forecasting future MRI, i.e., modeling the disease progression at the image level, is helpful in practice. For example, the forecasted image can allow clinicians to predict the possible progression speed by measuring the baseline and estimated MRI. It also can be shown to patients and their families when clinicians are providing advice and reassurance. The visualization of possible changes of brain may improve patients' trust in doctors and motivate their behavior, such as cognitive exercise.

In more recent years, benefit from the boost of generative adversarial network (GAN) [30], GAN-based methods have been adopted in various tasks, such as image registration, reconstruction, and segmentation [31]. Generally, the GAN model consists of a generator and a discriminator. They are trained in an adversarial way against each other, i.e., generator tries to generate synthetic image that discriminator cannot distinguish it from the real one. The adversarial mechanism in GAN can promote discriminator to generate more realistic image than conventional autoencoder [32]. To model disease progression at the image level, several studies have harnessed the GAN model to estimate brain MRI in the future [33–37], which can be regarded as an image synthesis task. For example, Bowles *et al.* [33] have modified the Wasserstein GAN with the image arithmetic technique in a latent space to directly manipulate the MRI of hippocampus, temporal lobe and the lateral ventricles. Ravi *et al.* [34] have trained a set of support vector regressors to capture the regional intensity change patterns before training GAN to produce two-dimensional MRI slice associated with disease progression.

However, the aforementioned researches have either focused on the cognitive score prediction or MRI image prediction when modelling the disease progression, without the consideration of the inherent correlation or relationship between these two views [38–40]. Besides, it is unknown that whether these two tasks can promote each other. In this study, we introduce a new solution to tackle this problem, with the overarching goal of predicting the future cognitive score and 3D MRI at the same time. Specifically, an end-to-end integrated framework for multi-view prediction of disease progression is proposed, by joint learning of the regression and GAN models. In this way, with the direct inputting of the whole-brain MRI once only, the integrated framework can predict subject-specific future MMSE and ADAS-cog scores and 3D MRI simultaneously. It not only accomplishes the main task of cognitive score prediction, but also achieves the auxiliary task of MRI prediction, which may provide more visualized complementary information, facilitating clinical decision-making and further enhancing the understanding of AD progression.

Obvious brain changes occur in some vulnerable regions, such as the

hippocampus and entorhinal cortex, which are crucial for the prediction of AD disease progression [41]. And clinicians also focus on analyzing these brain regions to make the diagnosis. For example, the whole brain and hippocampal atrophy rates are sensitive biomarkers of AD progression, and the atrophy degree of medial temporal structures is a diagnostic biomarker for AD [41]. Hence, these regions should be paid more attention to. In this study, we introduce a region-of-interest (ROI) loss to guide the training of the model. Specifically, based on the anatomical prior knowledge of AD, a 3D binary ROI mask that incorporates hippocampus, entorhinal cortex, amygdala, and other important regions is built [29,41,42]. Then, besides the baseline MRI, the ROI mask is also inputted into generator. Finally, the ROI loss, i.e., mean square error loss of ROIs, is constructed to guide generator to synthesize more realistic 3D MRI, especially in the ROI region. In summary, the main contributions of this work are three-fold.

- (1) The proposed end-to-end integrated framework unifies the regression model and the GAN model together to model AD progression in multi-view by predicting the future clinical scores and 3D MRI concurrently.
- (2) Three strategies for integrating the regression and GAN models are exploited, including the integration in generator, integration in discriminator, and integration in parallel with discriminator.
- (3) The ROI loss is proposed to guide the GAN model to generate high-quality MRI image and help to improve the prediction performance of the regression model, by leveraging the prior knowledge of AD.

2. Methods

The overview architecture of the end-to-end integrated framework is presented in Fig. 1. The 3D MRI of an individual at the baseline time-point (BL) is fed into the generator to predict MRI image at a future follow-up. The predicted or the real future MRI is inputted into the discriminator to identify its reality. The GAN is trained by the adversarial loss and the mean square error loss, while the region-of-interest-attentive generative adversarial network (ROI-GAN) is trained with an additional ROI loss (i.e., L_{ROI} shown in Fig. 1). It is the mean square error between the real and the generated ROI regions, obtained after performing element-wise multiplication with the ROI mask, respectively. Moreover, the regression model aims to simultaneously predict MMSE and ADAS-cog cores at the future time-point. It could be connected to the GAN model in three ways, shown as *Reg1*, *Reg2* and *Reg3* in Fig. 1. More details are provided in the following subsections.

2.1. Integrated frameworks for multi-view prediction

Inspired by [43–46], we propose the end-to-end integrated framework to forecast disease progression of AD in multi-view, i.e., predicting the 3D MRI and two cognitive scores simultaneously. We construct the regression model (regressor) and the GAN model to forecast two cognitive scores and MRI, respectively. In this section, we introduce three schemes to integrate the two models. First, we integrate them by taking the output features of bottleneck layer of generator as the input features of *Reg1*, named as the integration in generator (GAN_*Reg1*). Second, we integrate them by taking the output features of the last convolutional layer of discriminator as the input features of *Reg2*, named as the integration in discriminator (GAN_*Reg2*). They are feature-based integrated strategy, by leveraging the learned feature maps of the GAN model. Third, we integrate them directly and sequentially, by taking the output image of generator as the input image of *Reg3*. This is an image-based integrated strategy, named as the integration in parallel with discriminator (GAN_*Reg3*).

2.1.1. Integration in generator

Cao *et al.* [43] completed joint hippocampus segmentation and

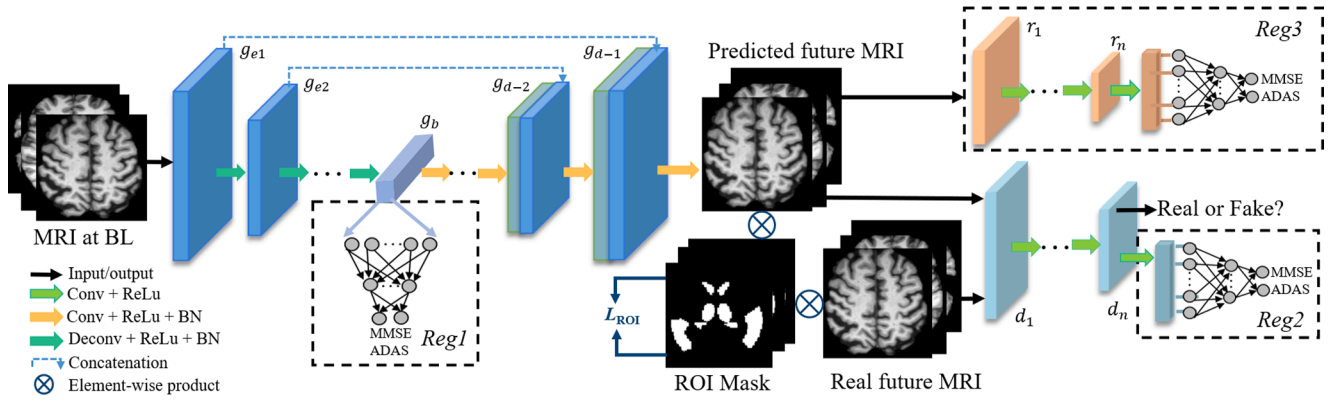


Fig 1. The overview architecture of the proposed end-to-end integrated framework. It integrates the regression model and the region-of-interest-attentive generative adversarial network (ROI-GAN) into a unified framework to predict 3D MRI and cognitive scores simultaneously. ROI-GAN consists of the generator ($g_{e1}, g_{e2}, \dots, g_{d-1}, g_d$) and the discriminator (d_1, \dots, d_n). The ROI loss, i.e., L_{ROI} is obtained by calculating the mean square error between the real and the generated ROI regions, after performing element-wise multiplication between the pre-defined 3D ROI mask and the real and the generated whole brain images, respectively. Three integrated strategies of the regression model, i.e., *Reg1*, *Reg2* and *Reg3* are shown in the black dash boxes respectively, to predict subject-specific cognitive scores at the future time-point. The cognitive scores include the mini-mental state examination score (MMSE) and Alzheimer's disease assessment scale cognitive subscale (ADAS-cog).

clinical score regression by connecting a regression model to the bottleneck layer of a segmentation model. Inspired by [43], to exploit the underlying correlation between the two predictions, we connect our regression model (*Reg1*) to the bottleneck layer of the GAN model by sharing the encoder ($g_{e1}, g_{e2}, \dots, g_b$) path. The feature maps from the bottleneck layer (g_b shown in Fig. 1) of generator are high-order features. Features in this latent space can reflect the mapping between the baseline image and the ground truth image to some degree. We input these features into the first layer of *Reg1* and then train the GAN and *Reg1* models jointly. The GAN loss and the regression loss can be formulated as:

$$L_{GAN}(G, D) = \mathbb{E}[\log D(Y)] + \mathbb{E}[\log(1 - D(G(X)))] + \alpha \mathbb{E}[\|G(X) - Y\|] \quad (1)$$

$$L_{Reg1}(R_1) = \mathbb{E}[\|R_1(g_b) - y\|] \quad (2)$$

where $X \in \mathbb{R}^{d \times w \times h}$ and $Y \in \mathbb{R}^{d \times w \times h}$ denote the MRI images, at baseline and the future time-point, respectively; and $\alpha > 0$ is a tunable hyper-parameter to balance the importance of adversarial loss and mean square error (MSE) loss. g_b is the bottleneck feature of generator, and y is the target score of future MMSE and ADAS-cog. To optimize them jointly, the total loss of this integration (L_{G_Reg1}) is:

$$L_{G_Reg1} = L_{GAN}(G, D) + \gamma L_{Reg1}(R_1) \quad (3)$$

where $\gamma > 0$ is a tunable hyper-parameter to balance the losses of GAN and *Reg1* models.

2.1.2. Integration in discriminator

Li et al. [44] appended an auxiliary fully connected network to the top of discriminator to predict the age of the face image when performing age progression and regression simultaneously. The fully connected network works as the regression model to predict the age of synthetic face image. Inspired by [44], to exploit the underlying relationship between the prediction of future MRI and clinical scores, we integrate our regression model (*Reg2*) and GAN model by inputting the extracted features (d_n as shown in Fig. 1) from the top of discriminator to the first layer of *Reg2*. These representations extracted by the last convolutional layer of discriminator contain abundant information to distinguish the generated image from the ground truth, and can be beneficial for the prediction of future cognitive scores. In this way, the regression loss and the discriminator loss work together to extract the effective shared features through the gradient back-propagation. The total loss function of this integration (L_{D_Reg2}) is:

$$L_{D_Reg2} = L_{GAN}(G, D) + \gamma L_{Reg2}(R_2) \quad (4)$$

$$L_{Reg2}(R_2) = \mathbb{E}[\|R_2(d_n) - y\|] \quad (5)$$

where d_n denotes the feature extracted by D .

2.1.3. Integration in parallel with discriminator

It was proved that adding an independent regressor to the GAN model can decrease the entropy of the generated face images [45]. Lanfredi et al. [46] proposed a VR-GAN model to visualize the progression of chronic obstructive pulmonary disease with chest X-rays. The introduction of the regression model can characterize the disease severity when the GAN model generating X-ray image with the desired severity level. Motivated by [45,46], we integrate an independent *Reg3* (shown in Fig. 1) in parallel with discriminator and also followed with generator. Different from the goal of discriminator, *Reg3* aims to make the generator synthesize high-quality image that can be used to predict cognitive score as precisely as possible. The quality of the predicted MRI image can affect the prediction performance of *Reg3* through back-propagating the hybrid loss of GAN and *Reg3* models. The total loss function of this integration (L_{New_Reg3}) is formulated as:

$$L_{New_Reg3} = L_{GAN}(G, D) + \gamma L_{Reg3}(R_3) \quad (6)$$

$$L_{Reg3}(R_3) = \mathbb{E}[\|R_3(G(X)) - y\|] \quad (7)$$

where $G(X)$ denotes the predicted MRI image.

2.2. ROI-GAN based integrated framework

In the fields of natural language processing and computer vision, some attention mechanisms [47,48] have been exploited to improve the representation of interests. For example, convolutional block attention module (CBAM) [47] can tell the model 'what' and 'where' to attend, by emphasizing features along both the channel and spatial dimensions. However, learning a reasonably accurate attention map is still challenging, due to the intrinsic locality of convolution operation. Thus, there raises a question: why not directly tell the model what and where to focus?

To answer this question, the ROI-GAN is proposed. Specifically, we firstly construct a 3D ROI mask that contains the location, shape and size of these important brain regions, using the WFU PickAtlas toolbox [49], implemented in Matlab (The MathWorks Inc., MA, USA). The ROI mask is a 3D binary matrix with voxels labeled 1 inside and 0 outside. It

contains the hippocampus, para hippocampus gyrus, amygdala, middle temporal gyrus, caudate, postcentral gyrus, fusiform gyrus, olfactory and thalamus regions, defined according to the automatic anatomical labeling brain atlas [50]. Secondly, we construct a specific ROI loss (i.e., L_{ROI} shown in Fig. 1), computed as the mean square error between the real and the generated ROI regions, formulating as:

$$L_{ROI}(G) = \mathbb{E}[||G(X) \otimes X_m - Y \otimes X_m||] \quad (8)$$

where $X_m \in \mathbb{R}^{d \times w \times h}$ is the ROI mask, and \otimes represents the element-wise multiplication. In this way, the ROI mask is merged into the GAN model and then guide it to synthesize more realistic brain image.

Furthermore, we also integrate the ROI-GAN model with the regression model to improve the overall performance of the end-to-end integrated framework. Thus, the hybrid loss of the ROI-GAN based integrated framework is:

$$\min_{G,R} \max_D (L_{GAN}(G,D) + \beta L_{ROI}(G) + \gamma L_{Reg}(R)) \quad (9)$$

where $\beta > 0$ and $\gamma > 0$ are the balance hyper-parameters, and $L_{Reg}(R)$ is the regression loss that could be $L_{Reg1}(R_1)$, $L_{Reg2}(R_2)$ or $L_{Reg3}(R_3)$, as described in Eqs. (2), (5) and (7).

2.3. Network architectures

As shown in Fig. 2, the framework includes a GAN model and a regression model. The network architectures are designed based on previous related studies [33–38] and our experiments, with the consideration of image size, sample size, and task complexity. The GAN model constitutes the U-net [51] like generator and the CNN-based discriminator. In the encoding path of generator, five convolutional blocks are adopted, shown as g_e in Fig. 1. Each block contains a convolutional layer, a leaky ReLU layer and a batch normalization layer [52]. The kernel size, stride and feature dimensions of the first four convolutional layers are (4, 4, 4) [53], (2, 2, 2) and (64, 128, 256, 512), and the kernel size of the last convolutional layer is (5, 6, 5). Correspondingly, in the decoding path of generator, five deconvolutional blocks are used, shown as g_d in Fig. 1. Each block contains a deconvolutional layer, a batch normalization layer and a leaky ReLU layer. The devolution of the first deconvolutional layer is (5, 6, 5), and the stride and feature dimension of the last four deconvolutional block are (2, 2, 2) and (512, 256, 128, 64). The feature maps from the encoding process are copied and then concatenated with the that in the decoding process via skip connection, shown by the blue dash arrows in Fig. 1. Then, the output of U-net is fed into a convolutional layer with one $1 \times 1 \times 1$ spatial filter by a stride of 1. Discriminator receives the generated or the real images and determines whether they are real or fake. It contains four convolutional layers and leaky ReLU layers, and two fully connected

layers, without using batch normalization layer like [54]. The feature dimensions of each convolutional blocks are 32, 64, 128 and 256. The output nodes of fully connected layers are 1000 and 1, respectively. Then, a sigmoid function is adopted to transform the output of the final layer to the [0, 1] range value, indicating the probability of the input image being considered as real or fake.

The regression model connects to the GAN model by integrating them in generator, in discriminator and in parallel with discriminator. Since the first two integrations are feature-based strategies, their architectures are identical, shown as *Reg1* and *Reg2* in Fig. 1. We experimentally set four fully connected layers, with the node number of 1000, 100, 10 and 1, in the regression model for predicting each cognitive score. The last integration is the image-based strategy, and its architecture is similar to that of discriminator, shown as *Reg3* in Fig. 1, excepting for the difference in the fully connected layers.

2.4. Baseline methods

Two deep-learning based regression models are built to accomplish the standalone prediction of clinical score. One is *Reg1* and the other is *Reg3*, as shown in Fig. 1. Most of their architectures are similar, except for the feature dimension of *Reg1* is twice that of *Reg3*. Notably, we do not construct *Reg2* as the baseline model, because of its inputting features should be extracted by the discriminator when distinguishing the generated and real images and its architecture is similar to *Reg3*. The baseline MRI and the future MRI are respectively fed into and then used to train the baseline regression models of *Reg1* and *Reg3*.

In addition, two baseline GAN models are constructed to predict the future 3D MRI image independently. One is GAN model that has the similar generator and discriminator architectures as shown in Fig. 1, trained without using the ROI loss. The other is CBAM-GAN that embeds four and two CBAM modules into the generator and the discriminator of the above GAN model. As described above, CBAM [47] is a commonly used learnable attention mechanisms, which can sequentially infer attention maps along channel and spatial dimensions and then focus on more important regions.

3. Experiment

3.1. Subject collection

The Alzheimer’s Disease Neuroimaging Initiative (ADNI,adni.loni.usc.edu) is a longitudinal multicenter dataset. It aims to develop clinical, imaging, genetic, and biochemical biomarkers for the early detection and disease progression tracking of AD. In this study, we selected 210 subjects with complete 3T MRI data and clinical scores at BL, at the first time-point (Year 1) and the second time-point (Year 4) from the ADNI-GO and ADNI-2 projects. Please note that the data was incomplete at the

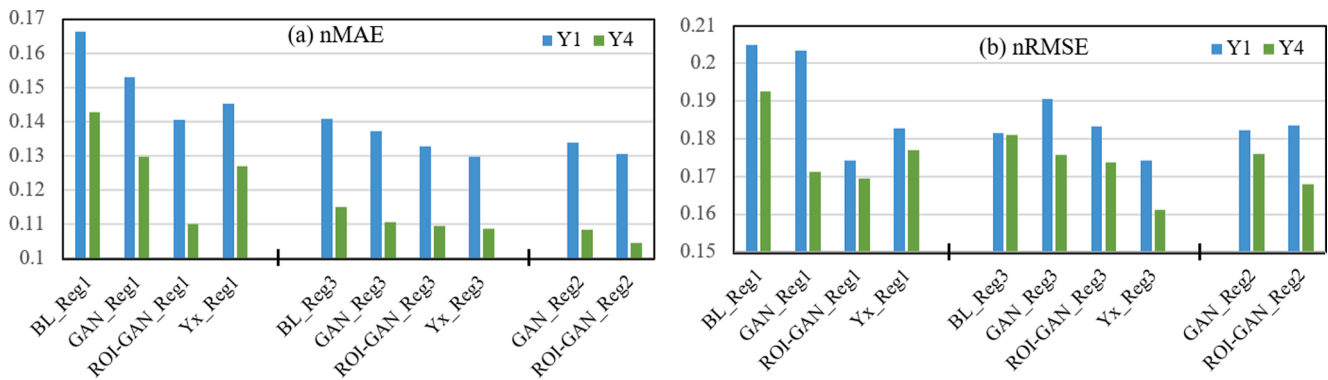


Fig. 2. Performance comparison of cognitive score prediction with different frameworks in terms of nMAE (a) and nRMSE (b). BL_Reg1 refers to the clinical score prediction using *Reg1* based on baseline MRI. Yx_Reg1 denotes the clinical score prediction using *Reg1* based on the real MRI image at two future follow-ups, i.e., year 1 (Y1) or year 4 (Y4). GAN_Reg1 and ROI-GAN_Reg1 represent the clinical score prediction using the GAN and ROI-GAN based integrated frameworks.

two and three years later from the baseline (205 subjects at Year 2 and 33 subjects at Year 3), so we did not consider these two time-points in this study. The demographic information of these 210 subjects is shown in Table 1.

3.2. Data preparation

Image preprocessing, such as brain extraction, normalization and registration, was performed on the raw MRI data to obtain the brain MRI with the size of $180 \times 192 \times 180$ [35]. Then, to reduce computation cost for GPU, down-sampling was performed to get the image with size of $90 \times 96 \times 90$. Furthermore, image augmentation [55] (e.g., rotation and shift) was performed on the training dataset. All of the clinical scores were also min-max normalized.

3.3. Implementation details

All experiments were implemented using the TensorFlow library, which was carried out on a NVIDIA Titan Xp 12 GB GPU. The subjects were randomly split into the training, validation and test datasets (3:1:1). The integrated framework was trained using the Adam optimizer with an exponential decay rate for the first moment of 0.5 and the mini-batch size of 6. The learning rate of the generator, discriminator and regressor were $1e^{-4}$, $1e^{-5}$, $1e^{-5}$, respectively. The hyperparameters were experimentally set to $\alpha = 100$, $\beta = 300$ and $\gamma = 1$. The number of training epochs was set to 200, and the training would stop if the prediction performance of the validation dataset was not improved in 10 epochs.

3.4. Evaluation

The end-to-end integrated framework can forecast the future 3D brain MRI and cognitive scores simultaneously. We used the root mean square error (RMSE) [17] to evaluate the prediction performance of each cognitive score, formulated as:

$$RMSE = \sqrt{\frac{\|y - \hat{y}\|_2^2}{n}} \quad (10)$$

where \hat{y} and y represent the predicted cognitive score (ADAS-cog or MMSE) and its corresponding ground truth, and n is the total number of subjects. Moreover, to show the overall performance of two scores, we compute the normalized mean index (nMI) by averaging the normalized mean absolute error (nMAE) and normalized RMSE (nRMSE). nMAE and nRMSE are computed after concatenating the normalized ADAS-cog and MMSE scores into one vector.

As for the image prediction, we adopted the mean squared error (MSE), the peak signal-to-noise ratio (PSNR), along with the structural similarity (SSIM) to assess the quality of the generated image [56]. These metrics can be calculated by:

$$MSE = \frac{1}{N} \|Y - \hat{Y}\|^2 \quad (11)$$

Table 1
Demographics of subjects at three time-points.

Time-point	NC/MCI/AD	AGE	ADAS-cog	MMSE
Baseline	76/134/0	71.32 ± 7.19	7.81 ± 3.87	28.47 ± 1.60
Year 1	81/119/10	72.34 ± 7.16	7.29 ± 4.51	28.10 ± 2.03
Year 4	86/87/37	75.43 ± 7.15	9.38 ± 7.68	27.06 ± 3.83

Notes: NC/MCI/AD means normal control, mild cognitive impairment or Alzheimer’s disease patient; MMSE and ADAS-cog denote mini-mental state examination score and Alzheimer’s disease assessment scale cognitive subscale. The data is presented in a mean ± standard deviation format.

$$PSNR = 10 \times \log_{10} \frac{MAXY^2}{MSE} \quad (12)$$

$$SSIM = \frac{(2\mu_Y \mu_{\hat{Y}} + C_1)(2\delta_{Y\hat{Y}} + C_2)}{(\mu_Y^2 + \mu_{\hat{Y}}^2 + C_1)(\delta_Y^2 + \delta_{\hat{Y}}^2 + C_2)} \quad (13)$$

where $Y \in \mathbb{R}^{d \times w \times h}$ and $\hat{Y} \in \mathbb{R}^{d \times w \times h}$ are the real and the generated images, and $N = d \times w \times h$ is the total voxels in the volumetric MRI image. Moreover, paired student’s t -test was utilized to show the performance difference between the GAN and ROI-GAN based models.

Apart from these quantitative measurements, we also qualitatively visualized the predicted MRI and the corresponding error map to reveal the difference between the predicted image and the ground truth. The error map is defined as:

$$error \ map = \begin{cases} 0, & |\hat{Y} - Y| < threshold \\ 1, & |\hat{Y} - Y| \geq threshold \end{cases} \quad (14)$$

where the threshold is a predefined value. If the voxel difference is less than the threshold, the error of this voxel is set to 0, otherwise set to 1.

4. Results

4.1. Better performance of clinical score prediction achieved with future MRI than baseline MRI

Given the baseline MRI, the quantitative performance of the two baseline regression models, *Reg1* and *Reg3*, for predicting the future MMSE and ADAS-cog scores was summarized in Table 2. We can observe that the *Reg3* model achieved better overall prediction performance than *Reg1*, and both models can yield better prediction performance based on the future MRI than that based on the baseline MRI image. For example, compared with BL_Reg1, obvious improvements were achieved by Y1_Reg1 and Y4_Reg1, e.g., the nMI values were decreased by 13.11% and 10.26%, respectively. These results demonstrated that the future MRI image can improve the prediction performance of the regression models. Thus, the prediction of the future MRI is valuable.

4.2. Better performance of MRI prediction achieved with ROI-GAN

To validate the effectiveness of the proposed ROI loss, three GAN models were constructed to predict the future 3D MRI image, including the GAN, CBAM-GAN and ROI-GAN models. The quantitative performance of these models was summarized in Table 3. It can be observed that our proposed ROI-GAN model outperformed the other two models on both prediction targets. For instance, compared with GAN for the task of predicting MRI image at Y4 (BL → Y4), our ROI-GAN model led to 8.79%, 0.05% and 1.12% improvements in terms of MSE, SSIM and PSNR for the ROI regions, and yielded 9.12%, 0.41% and 1.49%

Table 2
The results of clinical score prediction based on the real MRI images at two time-points.

Target	Framework	RMSE ↓ ADAS	RMSE ↓ MMSE	nMAE ↓	nRMSE ↓	nMI ↓
Year 1	BL_Reg1	4.1370	2.4206	0.1662	0.2048	0.1855
	BL_Reg3	3.9393	2.0722	0.1408	0.1815	0.1612
	Y1_Reg1	3.5953	2.1850	0.1452	0.1828	0.1640
Year 4	Y1_Reg3	3.6831	2.0159	0.1297	0.1742	0.1520
	BL_Reg1	6.3610	4.4189	0.1427	0.1925	0.1676
	BL_Reg3	7.2345	3.6192	0.1151	0.1809	0.1480
	Y4_Reg1	5.6965	4.1158	0.1269	0.1770	0.1520
	Y4_Reg3	6.3037	3.2978	0.1087	0.1613	0.1350

Notes: BL/Y1_Reg1/Reg3 denotes inputting the baseline MRI (BL) or real MRI at one year (Y1) and four years (Y4) later into *Reg1* or *Reg3* model. Boldface marks the best performance in the two tasks. ↓ means the lower the better.

Table 3

Performance of GAN models for 3D MRI prediction at two future time-points.

Target	GAN	Whole brain MRI ROI regions					
		MSE ($\times 10^{-3}$)↓	SSIM ↑	PSNR ↑	MSE ($\times 10^{-4}$)↓	SSIM ↑	PSNR ↑
BL → Y1	GAN	2.8353 ± 2.0624	0.9337 ± 0.0499	26.4983 ± 2.9647	3.5634 ± 2.7037	0.9928 ± 0.0055	35.6395 ± 3.2380
	CBAM-GAN	2.8666 ± 2.1193	0.9272 ± 0.0539*	26.5037 ± 3.0541	3.5968 ± 2.7511	0.9927 ± 0.0057	35.6345 ± 3.178
	ROI-GAN	2.7676 ± 2.0156*	0.9345 ± 0.0492**	26.6004 ± 2.9572*	3.4955 ± 2.6327	0.9929 ± 0.0054	35.7011 ± 3.1454
BL → Y4	GAN	3.0011 ± 1.8161	0.9291 ± 0.0459	25.8517 ± 2.2417	3.8308 ± 2.4867	0.9924 ± 0.0051	34.8568 ± 2.3349
	CBAM-GAN	2.8390 ± 1.9149*	0.9311 ± 0.0473**	26.2106 ± 2.4255**	3.6027 ± 2.6210*	0.9928 ± 0.0054*	35.2341 ± 2.4690**
	ROI-GAN	2.7502 ± 1.7680**	0.9329 ± 0.0460***	26.2372 ± 2.2078**	3.5213 ± 2.4535**	0.9929 ± 0.0052*	35.2456 ± 2.3269*

Notes: BL → Y1 and BL → Y4 denote the tasks of MRI image prediction at year 1 (Y1) and year 4 (Y4), given the MRI image at baseline (BL). Paired student's t-test (* $p < 0.1$, ** $p < 0.01$ and *** $p < 0.001$) is performed between the image prediction results of GAN and CBAM/ROI-GAN based frameworks. Boldface marks the best performance in the two tasks. ↑ means the higher the better, while ↓ means the lower the better.

improvements for the whole brain MRI. Compared with CBAM-GAN for the task of predicting MRI image at Y1 (BL → Y1), our ROI-GAN model led to 2.90%, 0.02% and 0.19% improvements in terms of MSE, SSIM and PSNR for the ROI regions, and yielded 3.58%, 0.79% and 0.36% improvements for the whole brain MRI. These results could indicate that the introduction of the knowledge-based prior can improve the performance of MRI image prediction.

4.3. Prediction performance of clinical score improved with joint prediction of future MRI

In this scenario, to assess whether the future MRI predicted by the integrated framework can improve the prediction performance of clinical score, GAN_Reg1 and GAN_Reg3 were constructed. Given 3D MRI of an individual at baseline, we predicted its future MMSE and ADAS-Cog scores and MRI concurrently. Their performance at the two follow-ups was listed in Table 4 and Fig. 2. Compared with BL_Reg1 and BL_Reg3 that fed baseline MRI into the regression model, the features learned by the generator (GAN_Reg1) and its predicted future MRI (GAN_Reg3) can improve the performance of clinical score prediction. Take the target of BL → Y1 for example, the nMI reduced from 0.1855 to 0.1574, with significant improvement.

Next, to further assess the benefit of ROI loss for the integrated framework, ROI-GAN_Reg1, ROI-GAN_Reg2 and ROI-GAN_Reg3 were also explored. Their performance was also shown in Table 4 and Fig. 2. Besides, we also listed their qualitative comparison for the image prediction in ROI regions in Table 5. These results demonstrated that the harness of ROI loss can improve the overall prediction performance of

Table 5

Performance comparison of GAN and ROI-GAN based integrated frameworks for MRI prediction in ROI regions.

Target	Framework	MSE (10^{-4})↓	SSIM ↑	PSNR ↑
BL → Y1	GAN_Reg1	4.4772 ±	0.9915 ±	34.6853 ±
	ROI-	3.4702	0.0060	3.2567
	GAN_Reg1	3.6020 ±	0.9928 ±	35.6999 ±
		2.7188***	0.0056***	3.0978**
	GAN_Reg2	3.5711 ±	0.9928 ±	35.6277 ±
	ROI-	2.7107	0.0055	3.1721
	GAN_Reg2	3.5255 ±	0.9929 ±	35.6293 ±
		2.6201*	0.0054*	3.0875
	GAN_Reg3	3.5920 ±	0.9928 ±	35.6107 ±
	ROI-	2.7351	0.0056	3.1855
	GAN_Reg3	3.5723 ±	0.9929 ±	35.6244 ±
		2.7126	0.0055*	3.1668
BL → Y4	GAN_Reg1	3.9617 ±	0.9920 ±	34.6741 ±
	ROI-	2.5981	0.0054	2.2591
	GAN_Reg1	3.7426 ±	0.9926 ±	35.0557 ±
		2.6870*	0.0055**	2.4587*
	GAN_Reg2	3.9050 ±	0.9924 ±	34.9012 ±
	ROI-	2.7570	0.0054	2.5364
	GAN_Reg2	3.6802 ±	0.9925 ±	35.1001 ±
		2.5320	0.0053	2.4640
	GAN_Reg3	3.8280 ±	0.9923 ±	34.9631 ±
	ROI-	2.6861	0.0055	2.5052
	GAN_Reg3	3.5798 ±	0.9928 ±	35.2533 ±
		2.5382***	0.0053***	2.4928***

Table 4

Performance of the proposed integrated frameworks for joint prediction of two cognitive scores and MRI.

Target	Framework	RMSE ↓	RMSE ↓	nMI ↓	MSE ($\times 10^{-3}$)↓	SSIM ↑	PSNR ↑
		ADAS	MMSE				
BL → Y1	BL_Reg1	4.1370	2.4206	0.1855	–	–	–
	GAN_Reg1	3.6309	2.5539	0.1781	3.4828 ± 2.6250	0.9270 ± 0.0528	25.6523 ± 3.0474
	ROI-GAN_Reg1	3.4358	2.0296	0.1574	2.8686 ± 0.0021***	0.9333 ± 0.0500***	26.4419 ± 2.9559**
	GAN_Reg2	3.7375	2.1378	0.1581	2.8384 ± 2.0650	0.9338 ± 0.0497	26.4885 ± 2.9535
	ROI-GAN_Reg2	3.7844	2.1478	0.1571	2.7944 ± 2.0001*	0.9341 ± 0.0487*	26.5223 ± 2.9005
	BL_Reg3	3.9393	2.0722	0.1612	–	–	–
	GAN_Reg3	3.8569	2.2490	0.1639	2.8577 ± 2.0956	0.9332 ± 0.0506	26.4788 ± 2.9854
	ROI-GAN_Reg3	3.7005	2.1656	0.1580	2.8376 ± 2.0005	0.9343 ± 0.0495***	26.4901 ± 2.9537
	BL → Y4	BL_Reg1	6.3610	4.4189	0.1676	–	–
GAN_Reg1		6.4687	3.6057	0.1506	3.0899 ± 1.8778	0.9287 ± 0.0466	25.6974 ± 2.1820
ROI-GAN_Reg1		6.2578	3.6277	0.1398	2.9683 ± 1.9951	0.9321 ± 0.0480**	26.0032 ± 2.3880*
GAN_Reg2		7.0679	3.5008	0.1422	3.1354 ± 2.0406	0.9303 ± 0.0470	25.7653 ± 2.4195
ROI-GAN_Reg2		6.5794	3.4301	0.1363	2.8672 ± 1.8365	0.9326 ± 0.0467*	26.1184 ± 2.3810
BL_Reg3		7.2345	3.6192	0.1480	–	–	–
GAN_Reg3		7.0324	3.5134	0.1433	3.0127 ± 1.9404	0.9269 ± 0.0488	25.9058 ± 2.3672
ROI-GAN_Reg3		7.2432	3.3225	0.1418	2.8245 ± 1.8442***	0.9299 ± 0.0470***	26.1975 ± 2.3820**

Notes: BL → Y1 denotes the task of future cognitive score and/or MRI image prediction at year 1 (Y1), given the MRI image at baseline (BL). BL → Y4 denotes the prediction at year 4 (Y4). BL_Reg1 represents the cognitive score prediction utilizing Reg1 model and taking the MRI image at BL as input. Y4_Reg3 represents the cognitive score prediction utilizing Reg3 model and taking the real MRI image at Y4 as the input. Paired student's t-test (* $p < 0.1$, ** $p < 0.01$ and *** $p < 0.001$) is performed between the results of GAN and ROI-GAN based frameworks. Boldface marks the best performance achieved by different frameworks for the two tasks. ↑ means the higher the better, while ↓ means the lower the better.

both clinical score and 3D MRI.

4.4. Visualization of the predicted MRI

In addition, we qualitatively evaluated the performance of our proposed GAN and ROI-GAN based integrated frameworks. Here, we took GAN_Reg1 and ROI-GAN_Reg1 as the example. The real and predicted MRI images of a subject (PTID: 019_S_4293) were displayed in Fig. 3. The MRI images in the first four columns seemed similar, and their differences look so trivial. Therefore, we also visualized the error maps between the real image and the predicted image at Y1 and Y4 in the last four columns of Fig. 3, respectively. These error maps illustrated that the quality of MRI predicted by the ROI-GAN based integrated framework was better than that predicted by the GAN based integrated framework, especially for the regions marked in red ellipse.

4.5. Performance compared with previous methods

This study has proposed a multi-task learning method to predict disease progression in multi-view, with the main prediction task of future two cognitive scores and the auxiliary prediction task of future 3D MRI. Thus, we mainly compared our methods with other traditional machine learning based [17,20] and artificial neural network based [19] approaches for predicting future scores. Comparison of the proposed integrated framework with other related works for predicting MMSE and ADAS-cog scores at one years later based on baseline MRI was shown in Table 6.

5. Discussion

In this study, we found that the prediction performance of future cognitive score achieved with future brain MRI was better than that with baseline MRI. To leverage the correlation between future brain MRI and future cognitive score, we presented an end-to-end integrated framework that can concurrently predict subject-specific cognitive score and future brain MRI. Experimental results on ANDI dataset showed (1) the integrated framework outperformed the independent regression model for cognitive score prediction; and (2) the integrated framework with ROI loss yielded better performance for both cognitive score and MRI

Table 6

Comparison of the proposed integrated framework with other related works for predicting MMSE and ADAS-cog scores at one years later based on baseline MRI.

Method	Subjects	Result (RMSE)
CSL [17]	130 AD, 295 MCI, 197 NC	MMSE 3.0705 ADAS-cog 6.0798
cFSGI [20]	133 AD, 304 MCI, 188 NC	MMSE 3.184ADAS-cog 5.678
APANN [19]	145 AD, 326 MCI, 198 NC	MMSE & ADAS-cog 7.10
SMTL [13]	91 AD, 202 MCI, 152 NC	MMSE 2.48 ADAS-cog 4.91
Ours	76 MCI, 134 NC	MMSE 2.8040 ADAS-cog 3.4358

prediction.

Cognitive score is common assessment to reflect the potential severity of AD, and its changing can model AD progression. Therefore, conventional studies [13–20,57] formulated the image-based AD progression as the regression task by predicting future cognitive scores. Recently, some studies [33–37] were formulated it as the image synthesis task by predicting future MRIs. Different from previous works that estimated the cognitive score or MRI independently, we attempted to construct an end-to-end integrated framework that can concurrently predict cognitive score and MRI, providing multi-view information for disease progression in one-pass way. Considering the heterogeneity of these tasks, how to integrate them together is challenging. Three strategies were exploited in [43–46] to unify two tasks for several applications, such as hippocampus segmentation [43], face image progression [44], and chronic obstructive pulmonary disease progression on chest X-rays [46]. However, which strategy is appropriate for our application is still unknown. In this work, we connected the regression and GAN models in three ways, and found that GAN_Reg2 performed better than GAN_Reg1 and GAN_Reg3. The reasons may be as follows. In GAN_Reg1, the shared feature may mainly concentrate on predicting the future MRI. In GAN_Reg3, the regression and GAN models maybe more concerned with their own primary targets. Whereas, in GAN_Reg2, the regression model shared the convolutional layers with the discriminator. Thus, the feature learned from the future MRI not only can be used to distinguish the predicted and real MRI, but also can facilitate the prediction of the cognitive scores. Therefore, we suggested that, in the longitudinal analysis, GAN_Reg2 may be more appropriate when both the regression and GAN models concentrate on the prediction of related tasks. Moreover, we innovatively incorporated expert knowledge into

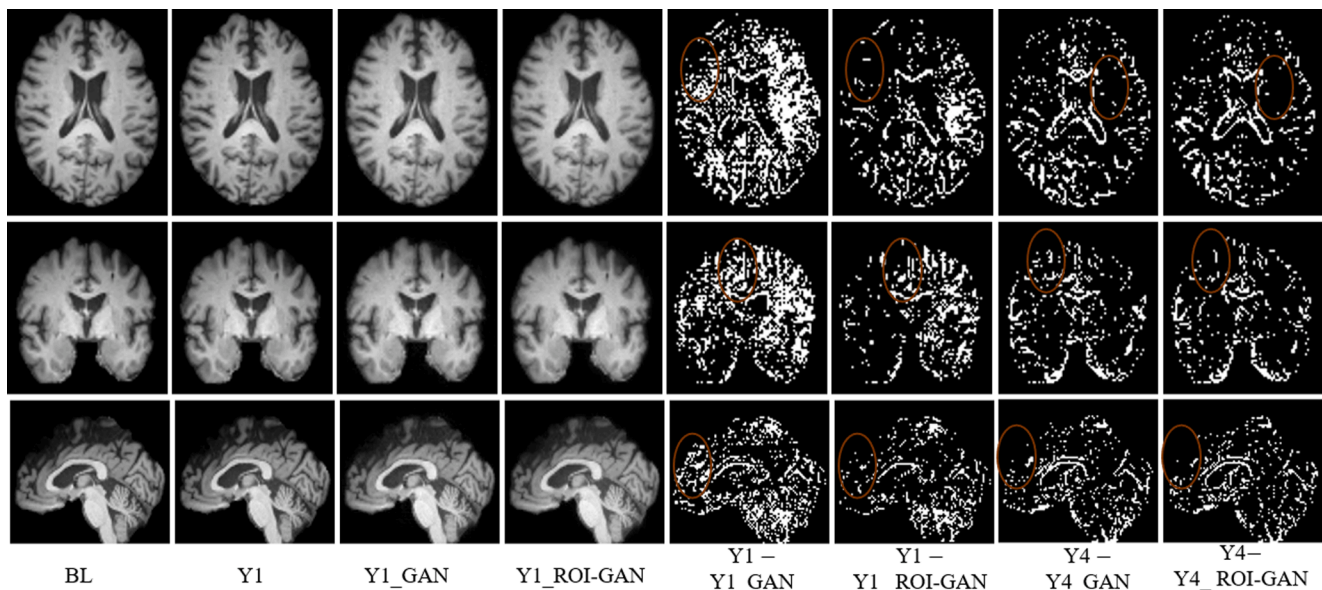


Fig. 3. Qualitive comparison of 3D MRI from the axial, coronal and sagittal views. The first and second columns show the real MRI images at baseline (BL) and one year later (Y1). The third and fourth columns are the MRI images predicted (shown as Y1_GAN and Y1_ROI-GAN) by the two integrated frameworks (GAN_Reg1 and ROI-GAN_Reg1). The last four columns are the error maps with the threshold of 0.06 between the predicted MRI images and the corresponding real MRI images at Y1 and Y4.

our integrated framework by adding a region-of-interest (ROI) mask and the corresponding ROI loss, which can guide the integrated framework focusing on the specific regions of brain to improve its learning capability.

Our current work has some limitations. First, the MRI image predicted by the integrated framework was inferior to that achieved by the independent GAN model. In this study, we experimentally set the network architecture for regression task and balanced the heterologous tasks in a hard way, which could lead to a scenario where one task had a dominant influence in the integrated framework, as shown in supplementary Tables S1 and S2. It may be better to automatically learn the optimal weights for different tasks when training. Some task-balancing techniques [58] or training strategies, such as dynamic weight average [59] and multi-phase training [60], may be beneficial for our framework. Second, our framework was validated with one dataset, and it can be extended to other longitudinal cohorts. Last but not the least, the opinion of some expert radiologists on our predicted MRI image should be consulted to promote its clinical application.

6. Conclusion

In this paper, we proposed an end-to-end integrated framework to forecast AD progression in multi-view, with the main task of cognitive score prediction and the auxiliary task of 3D MRI prediction. In this way, not only the potential disease severity of an individual can be predicted, but also the future informative MRI can be visualized in voxel-wise. Specifically, we integrated the regression and GAN models together and then trained them jointly. In addition, to leverage prior expert knowledge of disease progression, the 3D ROI mask and ROI loss were introduced into the integrated framework. Our experiments on the ADNI dataset demonstrated that the predicted MRI can significantly improve the prediction performance of the cognitive score, and ROI loss can further improve the prediction performance of both MRI prediction and cognitive scores.

CRedit authorship contribution statement

Yan Zhao: Conceptualization, Methodology, Data curation, Formal analysis, Software, Visualization, Writing - original draft. **Baoqiang Ma:** Software, Writing - review & editing. **Tongtong Che:** Resources, Writing - review & editing. **Qionglin Li:** Resources, Writing - review & editing. **Debin Zeng:** Resources. **Xuetong Wang:** Writing - review & editing. **Shuyu Li:** Funding acquisition, Supervision, Writing - review & editing.

Declaration of Competing Interest

The authors declare that they have no known competing financial interests or personal relationships that could have appeared to influence the work reported in this paper.

Acknowledgments

This work was supported by the National Natural Science Foundation of China (Nos. 81972160 and 81622025) and the Academic Excellence Foundation of BUAA for PhD Students.

Data collection and sharing for this project was funded by the Alzheimer's Disease Neuroimaging Initiative (ADNI) of United States, (National Institutes of Health Grant U01 AG024904) and DOD ADNI (Department of Defense award number W81XWH-12-2-0012). ADNI is funded by the National Institute on Aging, the National Institute of Biomedical Imaging and Bioengineering, and through generous contributions from the following: AbbVie, Alzheimer's Association; Alzheimer's Drug Discovery Foundation; Araclon Biotech; BioClinica, Inc.; Biogen; Bristol-Myers Squibb Company; CereSpir, Inc.; Eisai Inc.; Elan Pharmaceuticals, Inc.; Eli Lilly and Company; EuroImmun; F.Hoffmann-

La Roche Ltd and its affiliated company Genentech, Inc.; Fujirebio; GE Healthcare; IXICO Ltd.; Janssen Alzheimer Immunotherapy Research & Development, LLC.; Johnson & Johnson Pharmaceutical Research & Development LLC; Lumosity; Lundbeck; Merck & Co., Inc.; Meso Scale Diagnostics, LLC.; NeuroRx Research; Neurotrack Technologies; Novartis Pharmaceuticals Corporation; Pfizer Inc.; Piramal Imaging; Servier; Takeda Pharmaceutical Company; and Transition Therapeutics. The Canadian Institutes of Health Research is providing funds to support ADNI clinical sites in Canada. Private sector contributions are facilitated by the Foundation for the National Institutes of Health (www.fnih.org). The grantee organization is the Northern California Institute for Research and Education, and the study is coordinated by the Alzheimer's Disease Cooperative Study at the University of California, San Diego. ADNI data are disseminated by the Laboratory for NeuroImaging at the University of Southern California.

Appendix A. Supplementary material

Supplementary data to this article can be found online at <https://doi.org/10.1016/j.jbi.2021.103978>.

References

- [1] Z. Kh Ac Haturian, Diagnosis of Alzheimer's Disease, *Arch. Neurol.* 42 (11) (1985) 1097–1105.
- [2] C. Patterson, World alzheimer report 2018, 2018.
- [3] A.S. Association, 2019 Alzheimer's disease facts and figures, *Alzheimer's Dementia* 15 (3) (2019) 321–387.
- [4] D.P. Veitch, et al., Understanding disease progression and improving Alzheimer's disease clinical trials: Recent highlights from the Alzheimer's Disease Neuroimaging Initiative, *Alzheimer's Dementia* 15 (1) (2019) 106–152.
- [5] J.R. Cockrell, M.F. Folstein, Mini-mental state examination, *Principles and practice of geriatric psychiatry*, 2002, pp. 140–141.
- [6] S.T. Farias, et al., The measurement of everyday cognition (ECog): scale development and psychometric properties, *Neuropsychology* 22 (4) (2008) 531.
- [7] M.F. Folstein, S.E. Folstein, P.R. McHugh, "Mini-mental state": a practical method for grading the cognitive state of patients for the clinician, *J. Psychiatr. Res.* 12 (3) (1975) 189–198.
- [8] D. Galasko, M.R. Klauber, C.R. Hofstetter, D.P. Salmon, B. Lasker, L.J. Thal, The Mini-Mental State Examination in the Early Diagnosis of Alzheimer's Disease, *Arch. Neurol.* 47 (1) (1990) 49–52.
- [9] W.G. Rosen, R.C. Mohs, K.L. Davis, "A new rating scale for Alzheimer's disease," (in eng), *Am. J. Psych.* 141 (11) (Nov 1984) 1356–1364.
- [10] J.K. Kueper, M. Speechley, M. Montero-Odasso, "The Alzheimer's Disease Assessment Scale-Cognitive Subscale (ADAS-Cog): Modifications and Responsiveness in Pre-Dementia Populations. A Narrative Review," (in eng), *J. Alzheimers Dis.* 63 (2) (2018) 423–444.
- [11] B.M. Jernynak, et al., A computational neurodegenerative disease progression score: Method and results with the Alzheimer's disease neuroimaging initiative cohort, *NeuroImage* 63 (3) (2012) 1478–1486.
- [12] R.S. Doody, V. Pavlik, P. Massman, S. Rountree, E. Darby, W. Chan, Predicting progression of Alzheimer's disease, *Alzheimer's Res. Therapy* 2 (1) (2010) 2.
- [13] B. Lei, F. Jiang, S. Chen, D. Ni, T. Wang, "Longitudinal Analysis for Disease Progression via Simultaneous Multi-Relational Temporal-Fused Learning," (in English), *Front. Aging Neurosci. Orig. Res.* 9 (6) (2017).
- [14] M. Wang, D. Zhang, D. Shen, M. Liu, "Multi-task exclusive relationship learning for alzheimer's disease progression prediction with longitudinal data," (in eng), *Med. Image Anal.* 53 (2019) 111–122.
- [15] D.R. Mould, Models for Disease Progression: New Approaches and Uses (in English), *Clin. Pharmacol. Ther.* 92 (1) (2012) 125–131.
- [16] M. Nguyen, et al., "Predicting Alzheimer's disease progression using deep recurrent neural networks," (in eng), *NeuroImage* 222 (2020).
- [17] P. Jiang, X. Wang, Q. Li, L. Jin, S. Li, "Correlation-Aware Sparse and Low-Rank Constrained Multi-Task Learning for Longitudinal Analysis of Alzheimer's Disease," (in eng), *IEEE J. Biomed. Health Inform.* 23 (4) (Jul 2019) 1450–1456.
- [18] L. Huang, Y. Jin, Y. Gao, K.H. Thung, D. Shen, "Longitudinal clinical score prediction in Alzheimer's disease with soft-split sparse regression based random forest," (in eng), *Neurobiol. Aging* 46 (Oct 2016) 180–191.
- [19] N. Bhagwat, J. Pipitone, A.N. Voineskos, M.M. Chakravarty, "An artificial neural network model for clinical score prediction in Alzheimer disease using structural neuroimaging measures," (in eng), *J. Psych. Neurosci.* JPN 44 (4) (2019) 246–260.
- [20] J. Zhou, J. Liu, V.A. Narayan, J. Ye, "Modeling disease progression via multi-task learning," (in eng), *NeuroImage* 78 (Sep 2013) 233–248.
- [21] T. Abuhmed, S. El-Sa Pp Agh, J.M. Alonso, Robust hybrid deep learning models for Alzheimer's progression detection, *Knowl.-Based Syst.* 213 (4) (2020) 106688.
- [22] T. Jo, K. Nho, A.J. Saykin, "Deep Learning in Alzheimer's Disease: Diagnostic Classification and Prognostic Prediction Using Neuroimaging Data," (in English), *Front. Aging Neurosci. Syst. Rev.* 11 (220) (2019).

- [23] Y. LeCun, Y. Bengio, G. Hinton, Deep learning, *Nature* 521 (7553) (2015.) 436–444.
- [24] Y. Ding, et al., A Deep Learning Model to Predict a Diagnosis of Alzheimer Disease by Using 18F-FDG PET of the Brain, *Radiology* 290 (2) (2019) 456–464.
- [25] G. Litjens, et al., A survey on deep learning in medical image analysis, *Med. Image Anal.* 42 (2017) 60–88.
- [26] H. Choi, S. Ha, H. Kang, H. Lee, D.S. Lee, “Deep learning only by normal brain PET identify unheralded brain anomalies,” (in eng), *EBioMedicine* 43 (May 2019) 447–453.
- [27] C. Lian, M. Liu, L. Wang, D. Shen, Multi-Task Weakly-Supervised Attention Network for Dementia Status Estimation With Structural MRI, *IEEE Transactions on Neural Networks and Learning Systems*, 2021.
- [28] E.M. Reiman, et al., Brain imaging and fluid biomarker analysis in young adults at genetic risk for autosomal dominant Alzheimer’s disease in the presenilin 1 E280A kindred: a case-control study, *Lancet Neurol.* 11 (12) (2012) 1048–1056.
- [29] B.C. Dickerson, et al., “Alzheimer-signature MRI biomarker predicts AD dementia in cognitively normal adults,” (in eng), *Neurology* 76 (16) (2011) 1395–1402.
- [30] I. Goodfellow, et al., Generative adversarial nets, in: *Advances in neural information processing systems*, 2014, pp. 2672–2680.
- [31] X. Yi, E. Walia, P. Babyn, Generative adversarial network in medical imaging: A review, *Med. Image Anal.* 58 (2019) 101552.
- [32] S. Basu, K. Wagstyl, A. Zandifar, L. Collins, A. Romero, D. Precup, Early Prediction of Alzheimer’s Disease Progression Using Variational Autoencoders, Springer International Publishing, Cham, 2019, pp. 205–213.
- [33] C. Bowles, R. Gunn, A. Hammers, D. Rueckert, Modelling the progression of Alzheimer’s disease in MRI using generative adversarial networks, in: *Medical Imaging 2018: Image Processing*, vol. 10574, International Society for Optics and Photonics, 2018, pp. 105741K.
- [34] D. Ravi, D.C. Alexander, N.P. Oxtoby, A.S.D.N. Initiative, Degenerative adversarial neuroimage nets: Generating images that mimic disease progression, in: *International Conference on Medical Image Computing and Computer-Assisted Intervention*, Springer, 2019, pp. 164–172.
- [35] Y. Zhao, B. Ma, P. Jiang, D. Zeng, X. Wang, S. Li, Prediction of Alzheimer’s Disease Progression with Multi-Information Generative Adversarial Network, *IEEE J. Biomed. Health. Inf.* 25 (3) (2021) 711–719.
- [36] V. Wegmayr, M. Hörold, J.M. Buhmann, Generative Aging of Brain MR-Images and Prediction of Alzheimer Progression, in: *German Conference on Pattern Recognition*, Springer, 2019, pp. 247–260.
- [37] J. Bernal, S. Valverde, K. Kushibar, M. Cabezas, A. Oliver, X. Lladó, Generating Longitudinal Atrophy Evaluation Datasets on Brain Magnetic Resonance Images Using Convolutional Neural Networks and Segmentation Priors, *Neuroinformatics* (2021) 1–16.
- [38] N.C. Fox, R.I. Schill, W.R. Crum, M.N. Rossor, “Correlation between rates of brain atrophy and cognitive decline in AD,” (in eng), *Neurology* 52 (8) (1999) 1687–1689.
- [39] M. Dadar, R. Camicioli, S. Duchesne, D.L. Collins, “The temporal relationships between white matter hyperintensities, neurodegeneration, amyloid beta, and cognition,” (in eng), *Alzheimers Dement (Amst.)* 12 (1) (2020) e12091.
- [40] B.H. Ridha, et al., Volumetric MRI and cognitive measures in Alzheimer disease, *J. Neurol.* 255 (4) (2008) 567–574.
- [41] G.B. Frisoni, N.C. Fox, C.R. Jack Jr., P. Scheltens, P.M. Thompson, “The clinical use of structural MRI in Alzheimer disease,” (in eng), *Nat. Rev. Neurol.* 6 (2) (2010) 67–77.
- [42] H. Tabatabaei-Jafari, M.E. Shaw, E. Walsh, N. Cherbuin, Regional brain atrophy predicts time to conversion to Alzheimer’s disease, dependent on baseline volume, *Neurobiol. Aging* 83 (2019) 86–94.
- [43] L. Cao, et al., Multi-task neural networks for joint hippocampus segmentation and clinical score regression, *Multim. Tools Appl.* 77 (22) (2018) 29669–29686.
- [44] Q. Li, Y. Liu, Z. Sun, Age progression and regression with spatial attention modules, in: *Proceedings of the AAAI Conference on Artificial Intelligence*, vol. 34, no. 07, 2020, pp. 11378–11385.
- [45] S. Bazrafkan, P. Corcoran, Versatile auxiliary regressor with generative adversarial network (VAR+ GAN), arXiv preprint arXiv:1805.10864, 2018.
- [46] R. Bigolin Lanfredi, J.D. Schroeder, C. Vachet, T. Tasdizen, Adversarial Regression Training for Visualizing the Progression of Chronic Obstructive Pulmonary Disease with Chest X-Rays, in: *Medical Image Computing and Computer Assisted Intervention – MICCAI 2019*, Springer International Publishing, Cham, 2019, pp. 685–693.
- [47] S. Woo, J. Park, J.-Y. Lee, I. So Kweon, Cbam: Convolutional block attention module, in: *Proceedings of the European conference on computer vision (ECCV)*, 2018, pp. 3–19.
- [48] H. Tang, D. Xu, N. Sebe, Y. Yan, Attention-guided generative adversarial networks for unsupervised image-to-image translation, in: *2019 International Joint Conference on Neural Networks (IJCNN)*, IEEE, 2019, pp. 1–8.
- [49] J.A. Maldjian, P.J. Laurienti, R.A. Kraft, J.H. Burdette, An automated method for neuroanatomic and cytoarchitectonic atlas-based interrogation of fMRI data sets, *Neuroimage* 19 (3) (2003) 1233–1239.
- [50] N. Tzourio-Mazoyer, et al., Automated anatomical labeling of activations in SPM using a macroscopic anatomical parcellation of the MNI MRI single-subject brain, *Neuroimage* 15 (1) (2002) 273–289.
- [51] O. Ronneberger, P. Fischer, T. Brox, U-net: Convolutional networks for biomedical image segmentation, in: *International Conference on Medical image computing and computer-assisted intervention*, Springer, 2015, pp. 234–241.
- [52] S. Ioffe, C. Szegedy, Batch normalization: Accelerating deep network training by reducing internal covariate shift, in: *International conference on machine learning*, PMLR, 2015, pp. 448–456.
- [53] P. Isola, J. Zhu, T. Zhou, A.A. Efros, Image-to-Image Translation with Conditional Adversarial Networks, in: *2017 IEEE Conference on Computer Vision and Pattern Recognition (CVPR)*, 2017, pp. 5967–5976.
- [54] C.F. Baumgartner, L.M. Koch, K. Can Tezcan, J. Xi Ang, E. Konukoglu, Visual feature attribution using wasserstein gans, in: *Proceedings of the IEEE Conference on Computer Vision and Pattern Recognition*, 2018, pp. 8309–8319.
- [55] S. Shorten, T.M. Khoshgoftaar, A survey on image data augmentation for deep learning, *J. Big Data* 6 (1) (2019) 1–48.
- [56] U. Sara, M. Akter, M.S. Uddin, Image quality assessment through FSIM, SSIM, MSE and PSNR—a comparative study, *J. Comput. Commun.* 7 (3) (2019) 8–18.
- [57] T. Abuhmed, S. El-Sappagh, J.M. Alonso, Robust hybrid deep learning models for Alzheimer’s progression detection, *Knowl.-Based Syst.* 213 (2021), 106688.
- [58] S. Vandenhende, S. Georgoulis, W.V. Gansbeke, M. Proesmans, D. Dai, L.V. Gool, Multi-Task Learning for Dense Prediction Tasks: A Survey, *IEEE Transactions on Pattern Analysis and Machine Intelligence*, 2021, pp. 1–1.
- [59] A. Ghazipour, B. Veasey, A. Seow, A.A. Amini, Joint Learning for Deformable Registration and Malignancy Classification of Lung Nodules, in: *2021 IEEE 18th International Symposium on Biomedical Imaging (ISBI)*, 2021, pp. 1807–1811.
- [60] L. Liao, et al., Joint Image Quality Assessment and Brain Extraction of Fetal MRI Using Deep Learning, in: *Medical Image Computing and Computer Assisted Intervention – MICCAI 2020*, Springer International Publishing, Cham, 2020, pp. 415–424.